Investigation of clad ballooning during NSRR RIA tests using ALCYONE fuel performance code

Isabelle Guenot-Delahaie, Jerome Sercombe, Eric Federici, Christian Bernaudat, Rodrigue Largenton, Xavier Haller

Investigation of clad ballooning during NSRR RIA tests using ALCYONE fuel performance code

Isabelle Guénot-Delahaie[a,*], Jérôme Sercombe[a], Éric Fédérici[a], Christian Bernaudat[b], Rodrigue Largenton[c], Xavier Haller[d]

[a] CEA, DES, IRESNE, DEC, Cadarache F-13108 St-Paul-lez-Durance, France
[b] PRC/TC, EDF – DIPNN – DIRECTION TECHNIQUE, F-69007 Lyon, France
[c] Materials and Mechanics of Components Department (MMC), EDF R&D, F-77818 Moret-sur-Loing Cedex, France
[d] Framatome, F-69456 Lyon, France
* Corresponding author.
E-mail addresses: isabelle.guenot-delahaie@cea.fr (I. Guénot-Delahaie), jerome.sercombe@cea.fr (J. Sercombe), eric.federici@cea.fr (E. Fédérici), rodrigue.largenton@edf.fr (R. Largenton), xavier.haller@framatome.com (X. Haller)

Abstract

ALCYONE simulations of integral RIA transients performed on UO_2 fuel rods prior to or within the ALPS program in the Japanese NSRR facility with stagnant liquid water coolant conditions are presented in this paper. The 13 selected tests which cover a wide range of fuel enthalpy increases (200 J/g – 800 J/g) aimed at assessing/challenging ALCYONE capabilities on four quantities of interest: clad outer surface peak temperature (293 K – 1200 K), film boiling duration (0 s – 2 s), clad residual hoop strain (0% – 25%) and transient fission gas release (2% – 25%). Despite a global consistency between measurements and ALCYONE predictions, paths are investigated to explain and reduce discrepancies. In particular, the reevaluation of fuel enthalpies by JAEA has led to revisit ALCYONE clad-to-water coolant heat exchange models which were derived from previous values of fuel enthalpies and suggested a recalibration of some of their parameters. Then, modeling the delayed gas axial flow in the free volumes of the rod is shown essential to achieve better residual hoop strain predictions in case of clad ballooning if proper timing of fission gas release, rod internal pressure increase and clad temperature elevation can be simulated.

Keywords: PWR, RIA, NSRR, ALCYONE code, film boiling duration, clad ballooning, FGR, gas axial flow

1. Introduction

Co-developed within the PLEIADES software environment by CEA, EDF and Framatome, ALCYONE is a multidimensional finite element-based nuclear fuel performance code dedicated to the analysis of the behavior of fuel rods during irradiation in commercial Pressurized Water Reactors (PWRs), power ramps in experimental reactors or accidental conditions, including Reactivity-Initiated Accidents (RIAs). Capable of steady state and transient thermal modeling, ALCYONE solves fully-coupled equations of thermo-mechanics together with sophisticated models for fission gas swelling and release [1][2]. As regards RIA experiments, ALCYONE is capable of modeling the Pellet-Cladding Mechanical Interaction (PCMI) [2][3] and post-Departure from Nucleate Boiling (DNB) phases as well as various fuel/cladding material types. ALCYONE is in particular validated for PWR-UO_2 fuels with advanced claddings under “low pressure-low temperature” or “high pressure-high temperature” water coolant conditions [4] and for PWR-MOX fuels under sodium coolant conditions [5]. Current development work is focused on tests to be performed on high-burnup fuel rods under prototypical PWR conditions within the CABRI International Program [6] where heat transfer mechanisms related to transient boiling as well as Fission Gas Release (FGR) may induce clad failure by ballooning.

With a view to enlarging ALCYONE RIA validation base on water coolant tests and to test the code capability to reproduce clad ballooning, a selection of integral RIA transients performed on

UO_2 fuel rods in the Japanese NSRR facility with stagnant liquid water coolant conditions is considered in this paper. The reevaluation in 2014 of fuel enthalpies performed by the Japan Atomic Energy Agency (JAEA) led to the plot of several measures of interest as a function of the enthalpy increase during the tests [7,8]. Not only the measured clad outer surface peak temperature and film boiling duration were reported in the graphs, but also the maximum clad residual hoop strain and the transient FGR. Overall, this set of data gives a unique opportunity to challenge ALCYONE models related to clad-to-coolant heat exchanges, FGR and associated clad ballooning. One important aspect of NSRR tests is the often low initial internal pressure of the rodlet which makes clad ballooning unlikely if extensive FGR and local overpressure are not considered. The modeling of the high residual clad hoop strains (up to 25% locally) in some of NSRR tests is therefore a challenging task for any fuel performance code. Similar concerns were recently reported in the CSNI RIA synthesis reports [9,10] about the necessary improvement in fuel performance codes of models for clad-to-coolant heat transfer under very fast transients and transient boiling conditions, for fission gas dynamics, e.g. transient release and axial transport, and for cladding high-temperature mechanical behavior under RIA-relevant conditions.

In this paper, ALCYONE main features for pulse-irradiation simulation are first recalled with a focus on the modeling of the water boiling curve for RIA transient conditions. The selected NSRR tests to be simulated with ALCYONE are then presented. The comparison of the results from reference ALCYONE simulations with relevant experimental results (clad outer surface peak temperature and film boiling duration) are then discussed. A recalibration of the boiling curve parameters is proposed to reduce discrepancies between measured and calculated quantities. In the last part, calculated clad residual hoop strain and transient FGR are assessed and their sensitivity to the fuel permeability and to the FGR kinetics discussed.

2. NSRR tests

2.1. Description of the selected NSRR test cases

Among the RIA-simulation tests performed prior to or within the ALPS (Advanced LWR fuel Performance and Safety research) program by JAEA in the NSRR facility, a selection of 13 tests pertaining to the GK, HBO, TK, and RH-series related to PWR fuel rods are considered in this paper. To enlarge ALCYONE validation base, these 13 cases were chosen in order to encompass a wide range of rodlet and test characteristics, as well as measurement and examination results, among all information possible gathered through an up to date literature review [7,8],[11–41]. The main features of the selected integral tests are synthesized in Table 1. Compiled details are provided in Appendix A.

The fuel segments were extracted from either 17x17 or 14x14 lattice design PWR full-length fuel rods previously irradiated in different Japanese or European commercial reactors to high or very high burnup levels (38 – 67 GWd/tM is the range of local burnup achieved). They were composed of UO_2 fuel pellets sheathed with standard or low tin Zircaloy-4 or M5® advanced claddings. Refabricated with a more or less long pellet stack active length (50 to 135 mm), test fuel rodlets were more or less pressurized with helium (1 to 51 bar). Two types of experimental capsules are used in the NSRR facility, namely the Room Temperature (RT [1]) test capsule or the High Temperature (HT [1]) test capsule both with a stagnant water coolant initially at atmospheric pressure and room temperature or at high pressure (64 bar) and high temperature (280°C), respectively.

[1] RT and HT stand for « Room-Temperature, Atmospheric-Pressure » and « High-Temperature, High-Pressure » respectively.

Test pulses had a Full Width at Half Maximum (FWHM) around 4.4 ms for most of them and yielded radial average peak fuel enthalpy increase within a wide range (200 to 800 J/g). Some of the selected tests exhibited departure from nucleate boiling and film boiling during a few seconds leading to a cladding temperature excursion following the power pulse. Tests resulted in a wide variety of determined by rod puncturing transient FGR (ranging from 5 to 26 %) and rodlet residual hoop strain (up to 25% as regards the local maximum). Nevertheless none experienced any clad failure.

Table 1
Main features of the selected integral tests.

Test ID.	Characteristics
GK-1, GK-2	RT capsule Varying initial inner pressure [0.1 – 4.3 MPa]
HBO-2, HBO-3, HBO-4	RT capsule Varying pulse FWHM [4.4 – 6.9 ms] Varying initial inner pressure [0.1 – 5.1 MPa] Very high transient FGR (around 20%)
TK-1, TK-4, TK-5, TK-6, TK-8, TK-9	RT capsule Large range of measured clad residual strain [0.3 – 25%]
RH-1, RH-2	Sibling rodlets RH-1 (RT capsule) and RH-2 (HT capsule) M5® cladding Very high burnup [67 GWd/tM]

RT: Room Temperature. HT: High Temperature. FWHM: Full Width at Half Maximum.

2.2. Synthesis of NSRR test measurements

For all the NSRR tests performed before 2014, the calculated peak fuel enthalpy increases have been recently reevaluated by JAEA [7,8]. This excludes the latest tests performed on M5® rods (RH-1 and RH-2). The reevaluated enthalpies were 10 to 65% higher than the original values. Graphs illustrating the evolution of the following four quantities of interest with the new peak enthalpy increases were provided by JAEA: clad outer surface peak temperature, film boiling duration, clad residual hoop strain and transient fission gas release. The data available for PWR fuel rods only are reproduced in Fig 1.

The graphs include a large number of tests that exceeds the 13 selected NSRR transients. Considering that the tests conditions are very similar (FWHM in particular), they give interesting trends that may be summarized as follows: peak clad temperature starts to rise after 400 – 500 J/g of enthalpy increase and reaches ~1200 K at 600 – 750 J/g, film boiling time seems to rise at a higher enthalpy level (600 J/g) and reaches a maximum of ~2 s at 750 J/g, the residual clad hoop strain presents two slopes with a slow increase up to 600 J/g, followed by a fast rise afterwards, characteristic of clad ballooning, FGR seems to increase with enthalpy increase but dispersion is very important. The dispersion is for some part related to the large range of fuel burnups tested in the NSRR facilities.

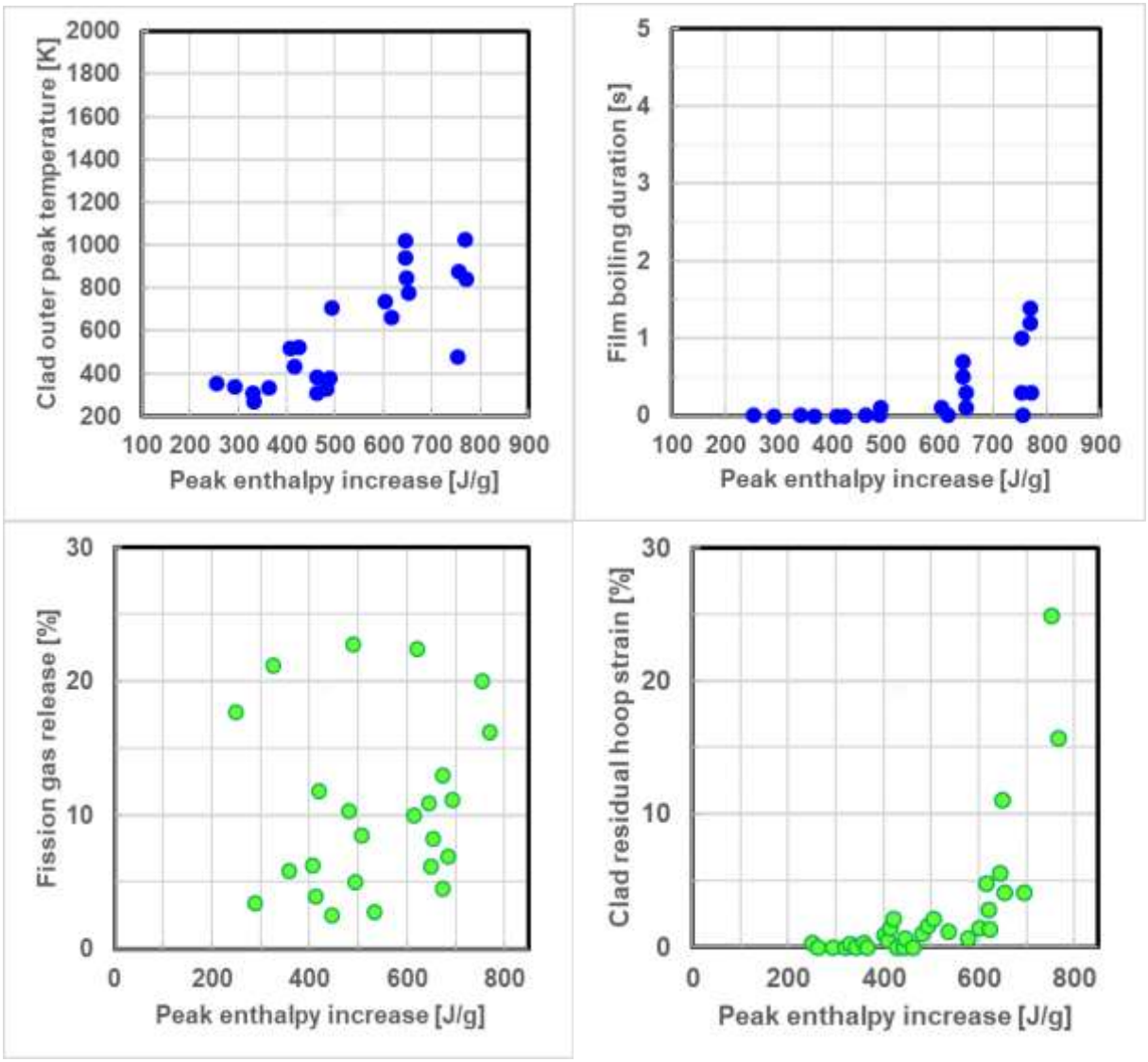

Fig 1. NSRR RIA test data for PWR fuel rods. Evolution *versus* reevaluated peak enthalpy increase of clad outer surface peak temperature (top left), film boiling duration (top right), transient fission gas release (bottom left) and clad residual hoop strain (bottom right). Adapted from [24].

In the next sections, ALCYONE main models will be described and simulation results will be compared to the measures gathered in Fig 1.

3. Outline of the fuel performance code ALCYONE

3.1. Main features

ALCYONE pulse-irradiation simulation capability includes (see details in [1,2,4,5]):

- the solving of the transient thermal heat balance equation and of the mechanical equilibrium for the pellet-gap-cladding system, based on the finite element method [42],
- the solving of the axial transient heat and mass balance equations for both sodium and water coolants. For NSRR stagnant water conditions under various pressure and temperature, the post-DNB stage is considered as will be detailed in the next part,

- material laws describing the non linear mechanical behavior of irradiated claddings (Zircaloy-4, M5® [2]) based on the extensive PROMETRA program performed on irradiated cladding samples submitted to high strain rates and high temperatures [43,44,45]. Based on a unified viscoplastic formulation (only one type of inelastic deformation) with no stress threshold between the elastic and viscoplastic regimes, these constitutive laws (see formulation in [46] and [47] for Zircaloy-4 and M5® respectively) aim at describing the anisotropic mechanical behavior of the (up to about 6 annual cycles) irradiated cladding material within large temperature (up to 1100°C for Zircaloy-4 and 820°C for M5®) and strain rate ranges (up to 5 s^{-1}),
- the modeling of grain boundary cracking and of the associated FGR occurring in UO_2 and MOX fuels (helium release can also be included in the simulation [48] since it can contribute to the increase of the fuel rod pressure). The onset and location of grain boundary cracking in the fuel pellet is given by the oxide fuel mechanical law that has been identified from compression tests performed on non irradiated samples at high strain rates and temperatures [49,50]. The amount of fission gases that is released from the regions where grain boundaries are cracked depends mostly on the precise assessment of fission gas partitioning prior to the RIA test, whether in inter- or intragranular position, in bubbles or dissolved, within the small grains and bubbles of the High Burnup Structure (HBS). It is given by a dedicated model called CARACAS which details can be found in [51]. An additional temperature criterion derived from annealing tests is considered as regards FGR from the HBS [52],
- the modeling of gas flow induced by axial pressure gradients inside the rod free volumes (including pellet dishes/chamfers/cracks and pellet-cladding radial gap, with their respective temperature) as an alternative to the more classical model assuming instantaneous equilibrium of pressure inside these volumes. It is mainly based on the ideal gas law and Darcy's law for gas flow under pressure P gradients within the rod considered as a porous medium characterized by its permeability K, following:
  $\frac{\partial}{\partial t}\left(\frac{\omega}{T}P\right) = \frac{d}{dz}\left(\frac{P}{T}\frac{K}{\mu}\frac{dP}{dz}\right) + R\dot{n}$ (Eq. 1)
  where $\frac{\omega}{T}$ stands for the gas storage capacity taking account of the different rod free volumes with their respective temperature, R is the universal gas constant, μ the gas dynamic viscosity and $\dot{n}$ the amount of gas released. It allows modeling the kinetics of gas axial redistribution in the fuel rod during a RIA transient that could explain localized clad ballooning observed in some NSRR tests,
- the accounting for the thermal resistance of outer zirconia depending on its thickness through a modification of the clad-to-coolant transfer coefficient (the zirconia thickness is currently not explicitly meshed).

One important feature of ALCYONE is the absence of any user-dependent specific initialization of the variables prior to pulse-irradiation simulations since the latter start from the base irradiation conditions that the code itself computes.

3.2. Boiling curves used in ALCYONE for water coolant and transient conditions

Solving the heat and mass balance equations requires the estimation of the heat flux between the clad outer surface and the water coolant. The clad-to-coolant heat flux is based on the boiling curves (i.e. heat flux *versus* clad temperature) proposed by Bessiron et al. [53][54] for PWR (150 bar, 280°C, 4 m/s) and NSRR (1 bar, room temperature, stagnant liquid water) conditions. The influence of the high heating rates involved in RIA is taken in the boiling curves into account, which renders the heat flux – temperature relation different from the one

[2] M5® is a trademark or registered trademark of Framatome or its affiliates, in the USA and other countries.

considered in steady state calculations, as shown in Fig 2-left. The transient boiling curve for the NSRR Room Temperature (RT) test conditions (1 bar) is illustrated in Fig 2-right. In ALCYONE, the heat flux derived from the different regimes is prescribed in the thermal calculation. An explicit time integration scheme is used with a strong constraint on the time step, in particular when the Critical Heat Flux (CHF) is reached. These developments have been tested successfully during the recent NEA RIA benchmark Phase II [55].

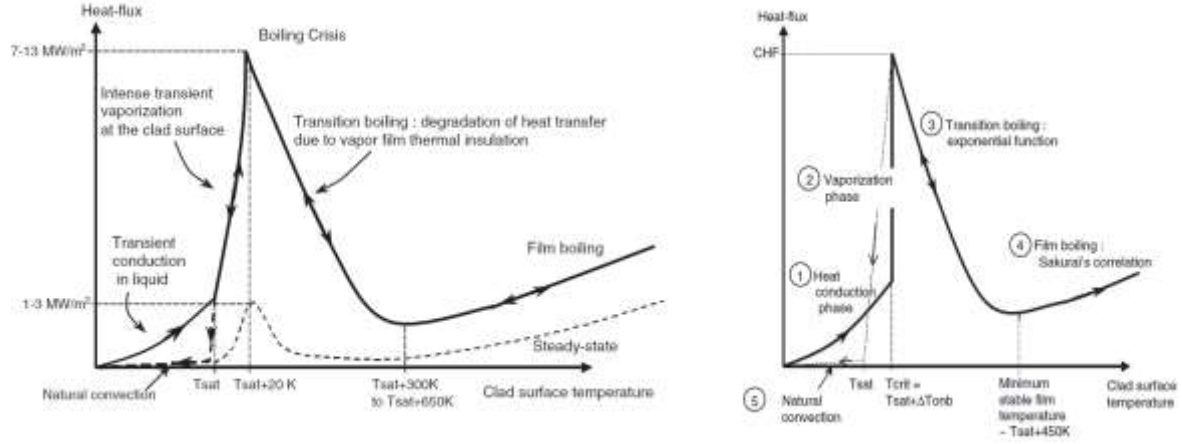

Fig 2. Clad-to-water heat transfer (reproduced from [54])
Left: schematic view of the experimental boiling curve in the NSRR tests (compared to the one in steady state conditions). Right: heat transfer regimes considered in the model.

As regards the simulation of NSRR RT tests, the correlations for stagnant liquid water conditions were derived by Bessiron from inverse analyses with the SCANAIR code [54][47][56] of NSRR tests performed on PWR pre-oxidized fresh fuel rods [57]. With Tsat denoting the saturation temperature, the transient boiling curve includes four different regimes (Fig 2-right):

- heat conduction in the stagnant liquid water up to the critical temperature (Tsat + 20 K),
- vaporization of a 30 μm thick layer (water thickness threshold denoted wtt in the following sections) of water at constant temperature (Tsat + 20 K). This regime was introduced to account for the impact of the energy deposition rate on the critical heat flux CHF,
  transition and film boiling regimes are simulated with a heat flux that decreases exponentially with the clad temperature up to Tsat + 450 K and then asymptotically tends to the film boiling heat flux estimated by Sakurai for steady-state conditions Φ^*_{SSH} [11]; the application to fast transients led Bessiron to introduce a multiplying factor k_B to best fit the NSRR tests [54] so that the heat flux in the film boiling regime follows:
  $\Phi = (\Phi_{crit} - \Phi_{SSH}) e^{\left[-k(T_{clad}-T_{crit})^2\right]} + \Phi_{SSH}$ (Eq. 2)
  where $\Phi_{SSH} = \mathrm{k}_B \Phi^*_{SSH}$. In ALCYONE, k_B = 5,
- the rewetting phase is activated when the temperature of the minimum heat flux is reached (Tsat + 450 K). The heat flux is calculated according to the same three previous correlations. This approach differs from the one proposed by Bessiron et al. [54] but was found to have little impact on the results [55].

As regards the simulation of NSRR High Temperature (HT) tests (64 bar, 280°C), neither the correlations derived by Bessiron for the NSRR RT tests nor the ones derived for the PWR cases from a series of experiments in the PATRICIA test loop of CEA [53] are applicable. A specific transient boiling curve adapted from the PWR model of Bessiron has nonetheless been implemented in ALCYONE. It includes the following four regimes:

- heat conduction in the stagnant liquid water up to the saturation temperature,

- a linear transition regime till the critical heat flux (6 MW/m²), between the saturation temperature and the critical temperature (Tsat + 55 K),
- a transition to the film boiling regime simulated by an exponential decaying function given by the following equation (similar to Eq. 2):
  $\Phi = \left(\Phi_{crit} - \Phi_{film}\right)e^{\left[-k(T_{clad}-T_{crit})^2\right]} + \Phi_{film}$ (Eq. 3)
  where the film boiling heat flux Φ_{film} is equal to 1.2 MW/m² consistently with the results of PATRICIA experiments and k = 3.10^{-4} K^{-2},
- the rewetting phase activated when the temperature of the minimum heat flux is reached. The heat flux is calculated according to the same three previous correlations.

4. ALCYONE simulations of selected NSRR tests

4.1. Assumptions and methodology

To be performed, any ALCYONE calculation requires input data including parent fuel rod and rodlet manufacturing data as well as the parent rod base irradiation and the rodlet pulse irradiation power histories. As regards the tests performed within JAEA NSRR programs, most of the data required for this study have been compiled from open-literature sources (see Appendix A) and completed as follows when data were missing.

Concerning base irradiation of the parent rods:

- for test cases GK-1 and 2, simplified base irradiation histories have been built on the basis of average linear heat generation rate data and number of cycles;
- for test cases RH-1 and RH-2, complete base irradiation histories were available in the CEA database;
- for test cases HBO-2, 3 and 4, and TK considered, the first cycles of some available base irradiation Linear Heat Rate (LHR) history of relevant (in terms of fuel and cladding materials and geometry) parent rods have been chosen to lead to consistent average rodlet burnups and outer zirconia layer thickness prior to the pulse test considered. Thus, within each series, tests with similar burnup may have been simulated with different power histories in case they had different outer zirconia thickness.

All the LHR histories considered during base irradiation are plotted in Fig 3. Note that the LHR range during the first cycle is important (150-300 W/cm).

Concerning pulse irradiation conditions:

- power pulse histories were built from the VA-3 test which detailed characteristics were available among the specifications of the 2013 phase I NEA benchmark [58]; the coupling factor was adjusted consistently with the peak fuel enthalpy increase achieved during the pulse test considered; the pulse FWHM was adjusted according to a time-scale expansion/contraction if needed (the Gaussian shape of the pulse is not changed);
- in case of lack of precise information about the axial power profile, it has been considered flat in ALCYONE simulations consistently with the LHR being almost uniform along the (short) pellet stack;
- for the latest tests RH-1 and RH-2, rodlet free volumes were available from post-test measurements of the free volume (4 cm^3 and 1 cm^3 respectively); for the other tests, estimations based on RH-1 and RH-2 rodlet free volumes have been used in ALCYONE calculations except for test cases GK-1 and 2, where a 1.5 cm^3 free volume has been considered. These choices have to be kept in mind since the free volume is an essential parameter with respect to clad ballooning.

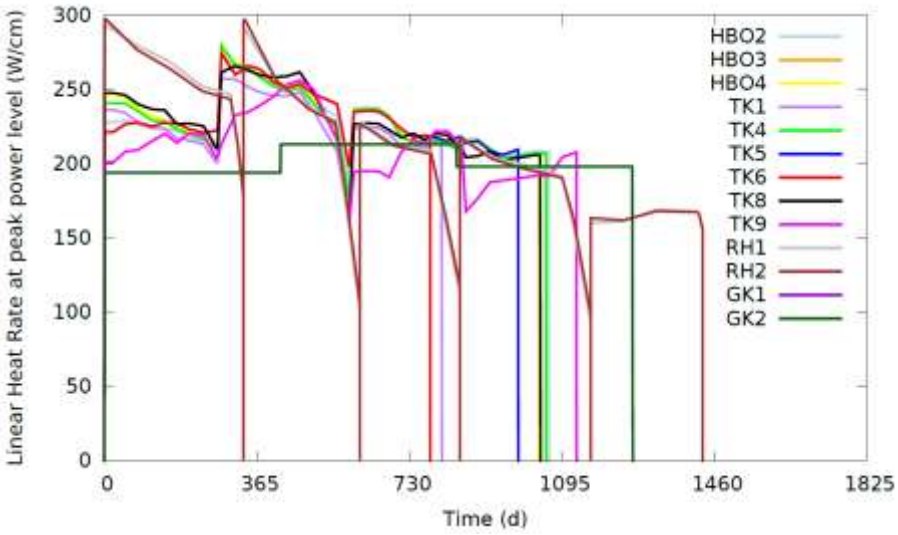

Fig 3. Time evolution of linear heat rate at peak power level considered in ALCYONE calculations

In a first set of ALCYONE calculations, pressure equilibrium in the rod free volumes is assumed, outer zirconia spallation is not considered. Complementary calculations accounting for zirconia spallation at starting time of the transient have been performed when it comes to comparing clad outer surface temperature results with measurements as will be detailed after.

4.2. Calculated average burnup, peak enthalpy increase and fission gas inventory

For the 13 tests selected, the ALCYONE calculated conditions characterizing both the end-of-base irradiation state (rodlet average burnup) and the transient pulse (enthalpy increase at peak power level, power evolution) are synthesized in Fig 4 and Fig 5, and compared to the values mentioned in the open literature. The wide ranges investigated for the burnup (high to very high) and for the mean enthalpy increase (between 250 and 750 J/g) as well as the small differences in pulse FWHM can easily be visualized.

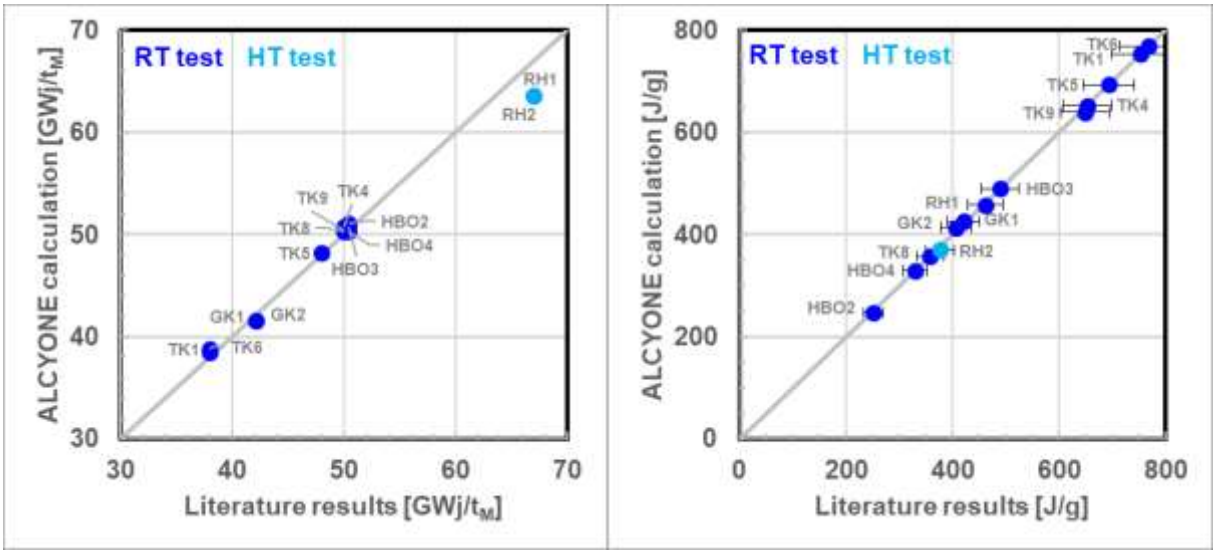

Fig 4. ALCYONE calculated *versus* literature values of (left) burnup and (right) peak enthalpy increase (symbols: dark blue for RT test, hell blue for HT test)

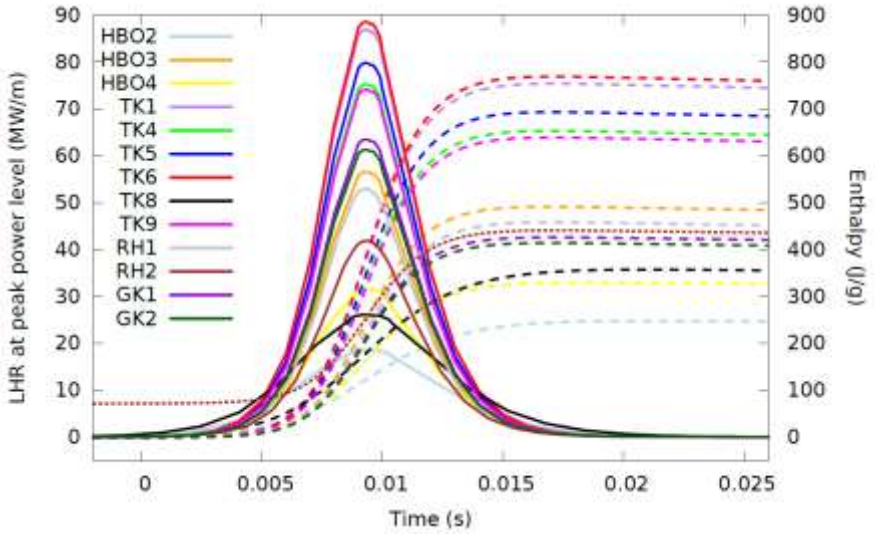

Fig 5. Time evolution of linear heat rate (left axis, solid line) and enthalpy (right axis, dashed line) at peak power level (N.B. LHR curves are centered on the same time only for representation purpose)

ALCYONE calculated FGR during base irradiation and the intergranular fission gas inventory before pulse testing are listed in Table 2. Fission gas release that occurred during base irradiation is excluded from the calculated pre-test intergranular fission gas inventory, which amounts between 15% and 20%. For some of the tests, base irradiation conditions lead to rather high release fractions under steady-state operation (around 4%). Within the HBO and TK series, differences in FGR during base irradiation between test cases having similar burnup are to be understood in the light of the differences in loading mentioned in section 4.1. For these series, the measured FGR during base irradiation (less than 0.5 %) is overestimated by ALCYONE. These results could be improved if more precise data on the pre-pulse base irradiation conditions and power histories were available. Nevertheless, the pre-test intergranular fraction in the fuel for the HBO series is high (18%), meaning that the overestimated FGR during base irradiation will not impact significantly the transient FGR. This is also the case for the TK series where the pre-test intergranular fraction reaches 15-18%.

Table 2
ALCYONE calculated burnup, FGR during base irradiation and pre-test rodlet intergranular fission gas inventory

Test ID.	Burnup (GWd/tM)	FGR during base irradiation (%[a])	Pre-test intergranular fraction (%[b])
GK-1	41.56	0.60	14.27
GK-2	41.56	0.60	14.27
HBO-2	51.11	4.54	18.31
HBO-3	50.82	3.77	17.72
HBO-4	50.35	3.60	17.50
TK-1	38.51	0.73	14.66
TK-4	50.82	3.77	17.72
TK-5	48.22	4.23	18.16
TK-6	38.77	2.00	17.02
TK-8	50.38	3.10	17.09
TK-9	50.39	1.81	16.22
RH-1	63.65	3.31	20.29
RH-2	63.6	3.33	20.38

[a] of the total amount of gas created within the fuel pellets.
[b] of the amount of gas retained within the fuel pellets after base irradiation.

4.3. Calculated clad outer surface peak temperature and film boiling duration

The following figures present results relative to the slice located at the maximum linear heat rate.

The instrumentation device of the NSRR tests includes thermocouples spot-welded on the clad, placed at one or several axial locations. Consistently with the removal of the oxidation layer below spot-welded thermocouples [59], the calculated time evolution of the clad outer surface temperature is plotted in Fig 6 assuming the spallation of the outer zirconia layer at starting time of the transient.

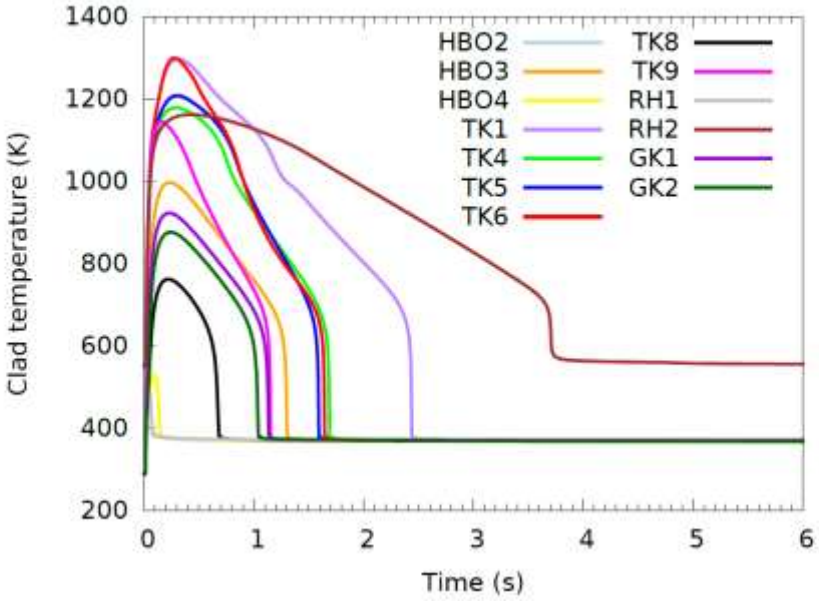

Fig 6. ALCYONE calculated time evolution of the clad outer surface temperature assuming the outer zirconia is totally spalled at the starting time of the transient

Fig 7 shows the calculated evolution of both clad outer surface peak temperature (left-hand) and film boiling duration (right-hand) *versus* peak enthalpy increase that can be compared to the graphs of Fig 1 (same x- and y-scales) where only the tests with M5® cladding are not represented. They are distinguished with grey circles in the graphs of Fig 7. Why they stand out from the tests performed on Zircaloy-4 rodlets is not related to their cladding material but rather a consequence of their higher burnup and of the water coolant pressure (70 bar) in the case of RH-2. Concerning RH-1, the calculated and measured film boiling durations are very low (close to 0) compared to sibling Zircaloy-4 rods (GK-1, GK-2, HBO-3) tested at the same enthalpy level. This might be due to the depleted thermal conductivity of the high burnup material which delays heat transfer with the coolant and hence the potential for DNB. Differences in external zirconia thickness are not important here since the simulation are run assuming zirconia spalling at the beginning of the transient.

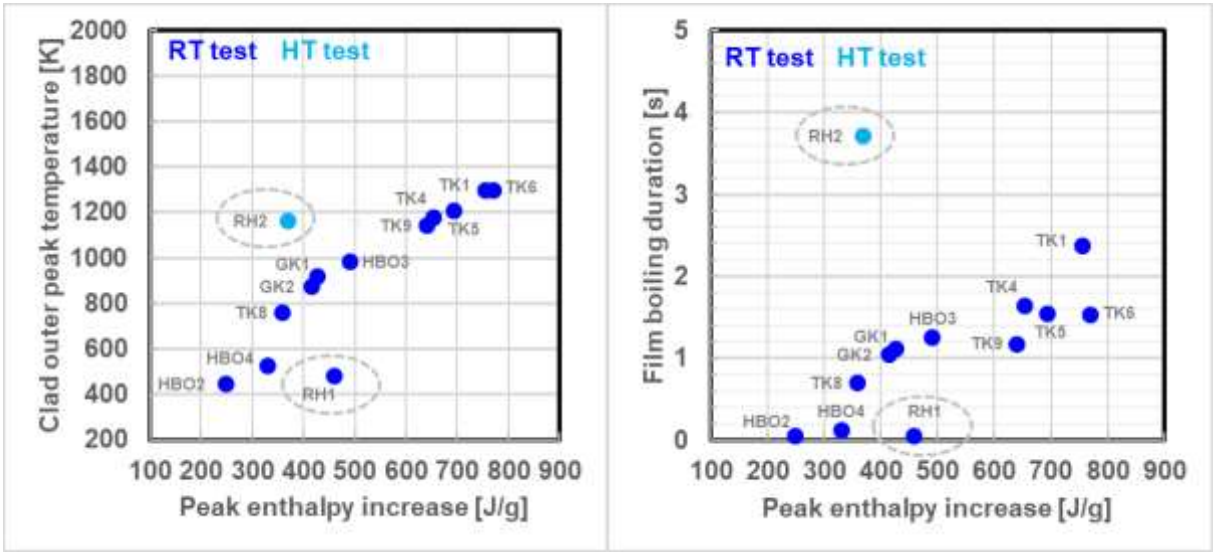

Fig 7. ALCYONE calculated values of clad outer surface peak temperature (left) and film boiling duration (right) *versus* peak fuel enthalpy increase (symbols: dark blue for RT test, hell blue for HT test)

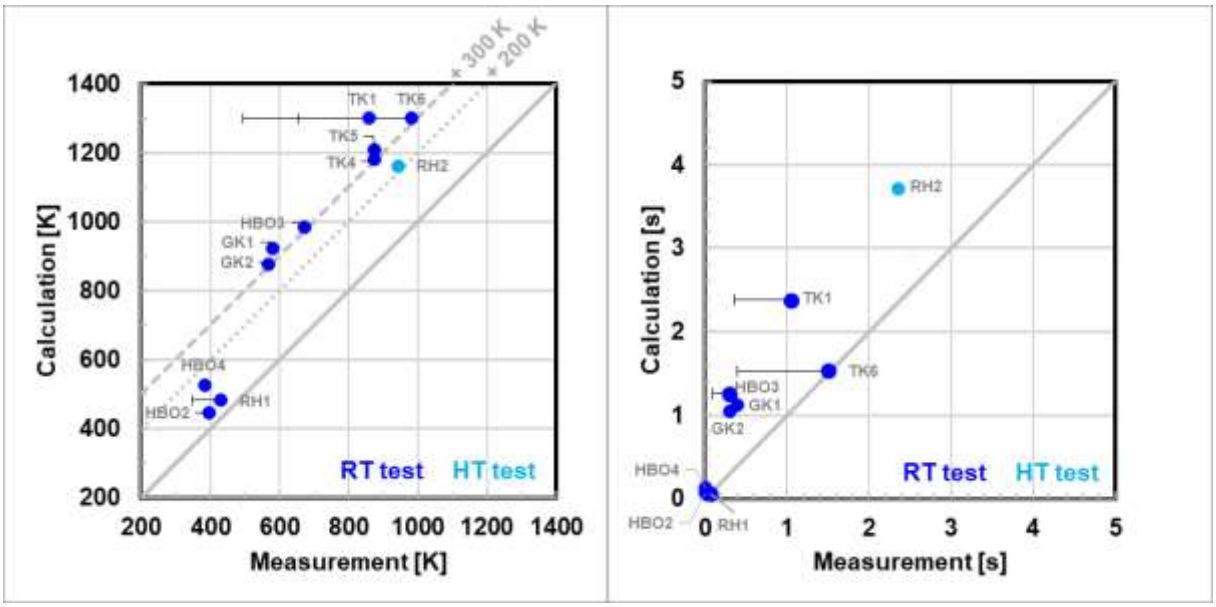

Fig 8. ALCYONE calculated *versus* measured values of (left) clad outer surface peak temperature and (right) film boiling duration (symbols: dark blue for RT test, hell blue for HT test)

To better evidence the discrepancies, Fig 8 compares ALCYONE calculated and measured values for both clad outer surface peak temperatures (left-hand) and film boiling durations (right-hand). At first sight, the calculated temperatures appear overestimated, especially when DNB occurs, but they are within the uncertainty of measurements (200 – 300 K) due to some thermocouple fin effect [60]. Whether irradiation contributes to the overestimation is not obvious (Bessiron's boiling curve was established from tests performed on virgin samples [54]). The order of magnitude of the calculated clad outer surface peak temperatures is thus considered correct and the general trend of Fig 1 recovered. ALCYONE calculations exhibit a steady increase of the clad outer surface peak temperature with peak enthalpy increase from a value of around 320 J/g. In Fig 1, the temperature increase occurs a bit later, at an enthalpy increase of 400-450 J/g.

Similarly, ALCYONE calculations of the film boiling duration exhibit a steady increase with peak enthalpy increase starting from around 320 J/g followed by a stabilization around 700 J/g. Although overestimated, and whether irradiation contributes to the overestimation is here again not obvious, the order of magnitude of the calculated film boiling duration (0 to 2.5 seconds) given by the clad-to-coolant heat exchange model in ALCYONE is considered correct. Nevertheless, when compared with the general trend exhibited in Fig 1, boiling occurrence seems overestimated which incidentally explains partly the overestimation of the clad outer surface peak temperature and questions the value of the critical heat flux considered.

Actually the clad outer surface peak temperature and film boiling duration have been determined from the models described in section 3.2 that have a large part of empiricism and need to be updated, especially since the reevaluation of the fuel enthalpies (10 to 65%) that took place in 2014 [7,8]. From an experimental point of view, Sugiyama reported for instance an increase by a factor of 4 of the film boiling duration induced by a variation of +50% in peak fuel enthalpy during tests performed on non-oxidized samples [57]. Given the current lack of experimental investigations on boiling heat transfer in RIA conditions [9], some readjustment of the heat transfer correlations sounds legitimate. It is the purpose of the next section.

4.4. Readjustment of the boiling curve parameters for NSRR tests

Sensitivity analyses have been performed on several parameters outlined in section 3.2.

As regards the correlations for NSRR RT tests, varying the water thickness that needs to be vaporized before the boiling crisis occurs denoted wtt had no obvious influence on the critical heat flux in the calculations, contrary to the heat flux at rewetting. The reference value of 30 µm has therefore been kept. Sensitivity analyses have shown that varying the parameter k_B around the reference value of 5 led in some case to a better prediction of film boiling durations and incidentally of peak clad temperatures. Given the known uncertainties on the clad temperature measurements (200 – 300 K), parameter fitting on the film boiling duration has been favored. A value of 8 has finally been retained.

As regards the correlations for the NSRR HT tests, varying the film boiling heat flux Φ_{film} around the reference value of 1.2 MW/m² has an interesting impact especially on the film boiling duration. A value of 1.5 MW/m² has finally been retained. Adopting a value of 10^{-4} K^{-2} for the decaying exponential parameter k instead of 3.10^{-4} K^{-2} proved also to be advantageous. Since film boiling is reached later, a higher injected energy is required.

Fig 9 shows ALCYONE calculated clad outer surface peak temperatures and film boiling durations *versus* measurements after readjustment of the boiling curves parameters. Compared to Fig 8, it evidences the global improvement for all the tests considered.

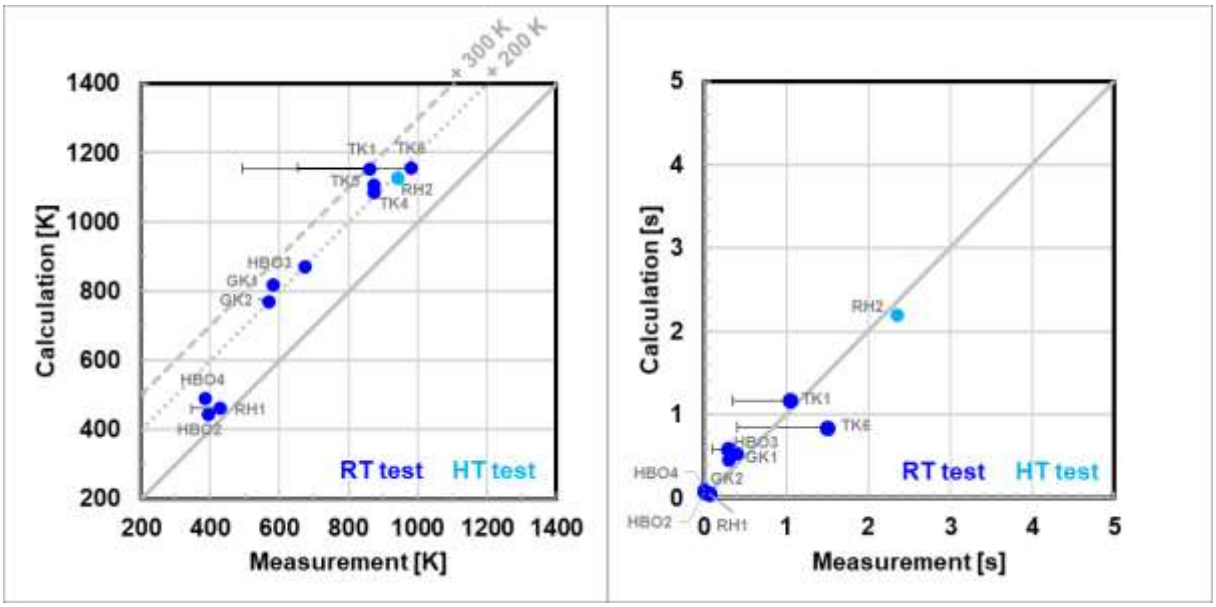

Fig 9. ALCYONE calculated *versus* measured values of clad outer surface peak temperature (left) and film boiling duration (right) after parameter fitting on k_B, k and Φ_{film}(symbols: dark blue for RT test, hell blue for HT test)

Fig 10 shows ALCYONE calculated clad outer surface peak temperatures and film boiling durations *versus* peak enthalpy increase after parameter fitting. The general trend when compared to Fig 7 is to lower temperatures and shorter film boiling durations. As the sensitivity analysis on parameter wtt did not show the expected influence on the value of critical heat flux, the overestimation of film boiling initiation around 300 J/g has not been improved.

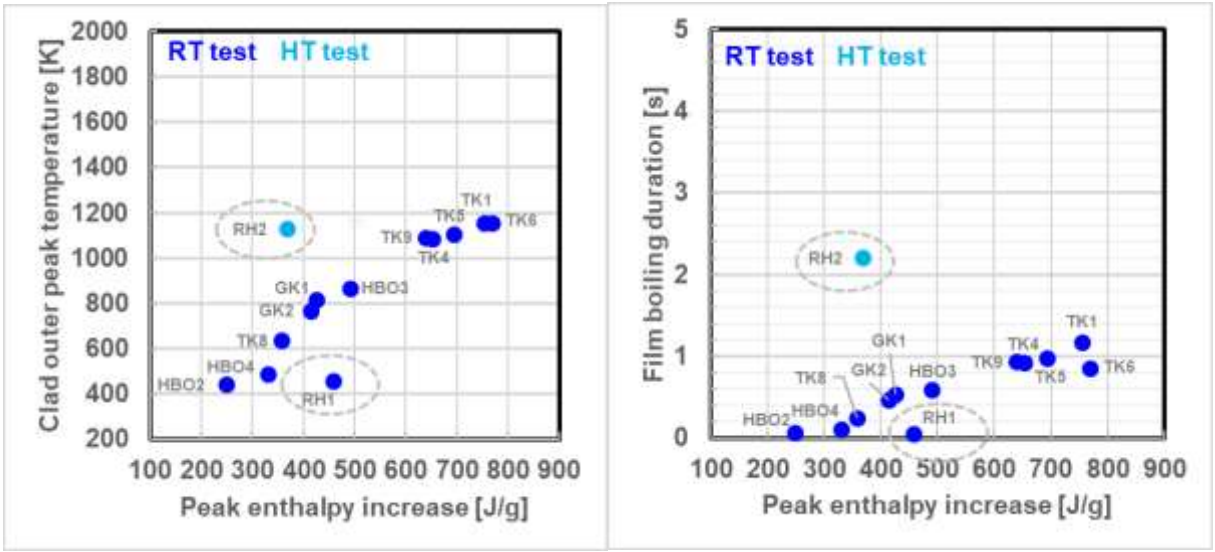

Fig 10. ALCYONE calculated values of clad outer surface peak temperature (left) and film boiling duration (right) *versus* peak enthalpy increase after parameter fitting on k_B, k and Φ_{film}(symbols: dark blue for RT test, hell blue for HT test)

4.5. Calculated transient FGR

Now that the thermal heat transfer parameters have been optimized, the calculated FGR can be discussed. Transient fission gas release refers to the incremental fission gas release during the pulse irradiation, exclusive of fission gas release during base irradiation.

Fig 11 shows calculated transient fission gas release *versus* peak enthalpy increase. The graph can be compared to Fig 1 where all the measurements available from NSRR RT tests are plotted. Having the same axes and the same scales, the two figures can thus be compared despite the fact that Fig 1 does not integrate rodlets with M5® cladding which are distinguished with grey circles in Fig 11. Fig 12 shows the comparison between ALCYONE calculation results and measurements.

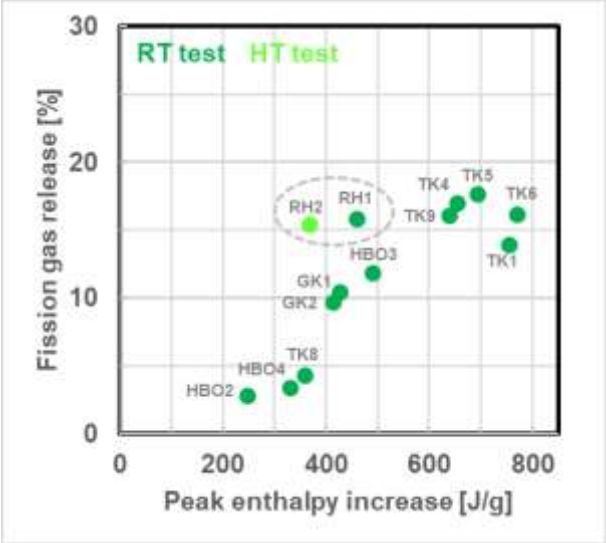

Fig 11. ALCYONE calculated results of transient fission gas release *versus* peak fuel enthalpy increase (symbols: dark green for RT test, hell green for HT test)

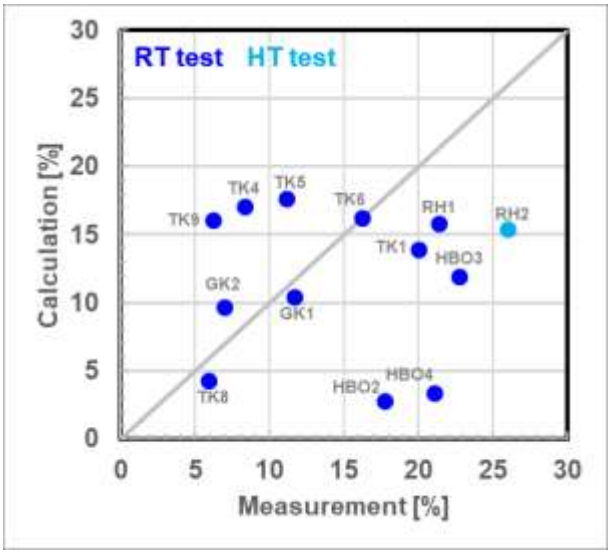

Fig 12. ALCYONE calculated *versus* measured values of transient fission gas release (symbols: dark blue for RT test, hell blue for HT test)

As shown in Fig 1, the experimental dispersion is significant. Nevertheless, keeping apart the few test cases showing a FGR of ~20% independently of the enthalpy increase, the general trend is that FGR globally increases with enthalpy increase above 300 J/g. ALCYONE calculations exhibit a similar trend with a steady increase of FGR with enthalpy increase till stabilization around a level consistent with the pre-transient intergranular gas inventory (around 20%, see Table 2).

Actually the pulse width is the main factor in the coupling used in ALCYONE between the fuel mechanical model and transient FGR. It determines the compressive stress level within the fuel pellet during the power increase part of the pulse which triggers grain boundary cracking (and FGR) in ALCYONE. It seems thus not surprising for example that the less energetic RH-2 test and the more energetic TK-1 test have equivalent FGRs (the FHWM is identical). As pointed out in the CSNI report [9], the HBO tests (2 and 4) present rather unexpected high FGR (17 and 22%) considering their moderate fuel enthalpy increase during the tests and the somewhat larger FWHM (7 ms). In spite of an intergranular inventory prior to the test that is not negligible (18%), ALCYONE simulations give fairly small FGR for these two tests (less than 5%). This can be explained as follows.

Following recommendations made in the recently updated CSNI state-of-the-art report on fuel behaviour under RIA conditions [9], Fig 13 shows the transient intergranular gas release (given by the ratio of the transient fission gas release to the pre-test intergranular fission gas fraction in the fuel, cf. Table 2) *versus* the ratio of peak fuel enthalpy increase to pulse width. This ratio was found to correlate better with FGR in the neural network study of NSRR tests by Koo et al. [41]. It is actually a measure of the pulse kinetics and hence of the thermomechanical stresses within the fuel pellets during the power increasing phase. An interesting trend in ALCYONE simulations can be observed, probably less scattered than the one obtained for transient FGR. Recalling that ALCYONE FGR is mostly driven by compressive stresses during the power increasing phase (and hence dependent on the pulse kinetics), this explains why the calculated FGR during the HBO tests are small. Obviously, another mechanism has to be taken into account during these tests if consistent FGRs are to be calculated. In the CSNI report [9], the high FGR are related to the development of fine radial cracks at the HBO pellets periphery. This tensile induced grain boundary cracking is not considered in ALCYONE yet. As expected from the small FWHM, ALCYONE calculations do not predict any intragranular gas contribution to the transient FGR (by gas bubble migration) since the transient intergranular FGR fractions are always lower than 100%.

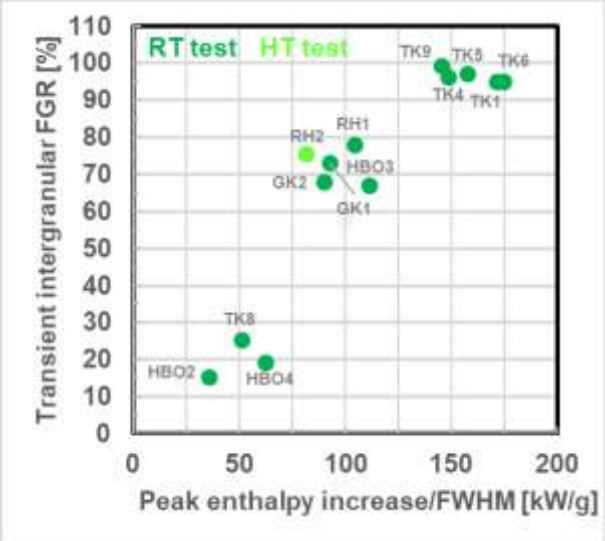

Fig 13. ALCYONE calculated results of transient intergranular fission gas release *versus* ratio of peak fuel enthalpy increase to FWHM (symbols: dark green for RT test, hell green for HT test)

4.6. Calculated clad residual hoop strains during pulse tests

Fig 14 shows the evolution of the clad residual hoop strain *versus* peak enthalpy increase as calculated by ALCYONE. This graph can be compared to the measures of Fig 1 that include

however more NSRR tests. As can be seen, the small database of 13 tests considered in this paper is sufficient to study the main trends observed in Fig 1. Fig 15 shows the comparison between ALCYONE calculation results and measurements of the clad residual hoop strains generated during the NSRR pulse tests. In this figure, ALCYONE calculated values are compared to the measured axially mean clad residual hoop strains if available. If not available, the measured axially maximum value is considered and plotted in red.

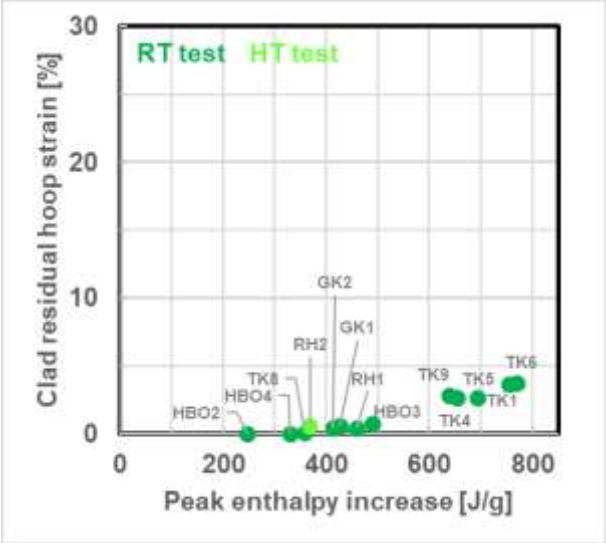

Fig 14. ALCYONE calculated results of clad residual hoop strain *versus* peak fuel enthalpy increase (symbols: dark green for RT test, hell green for HT test)

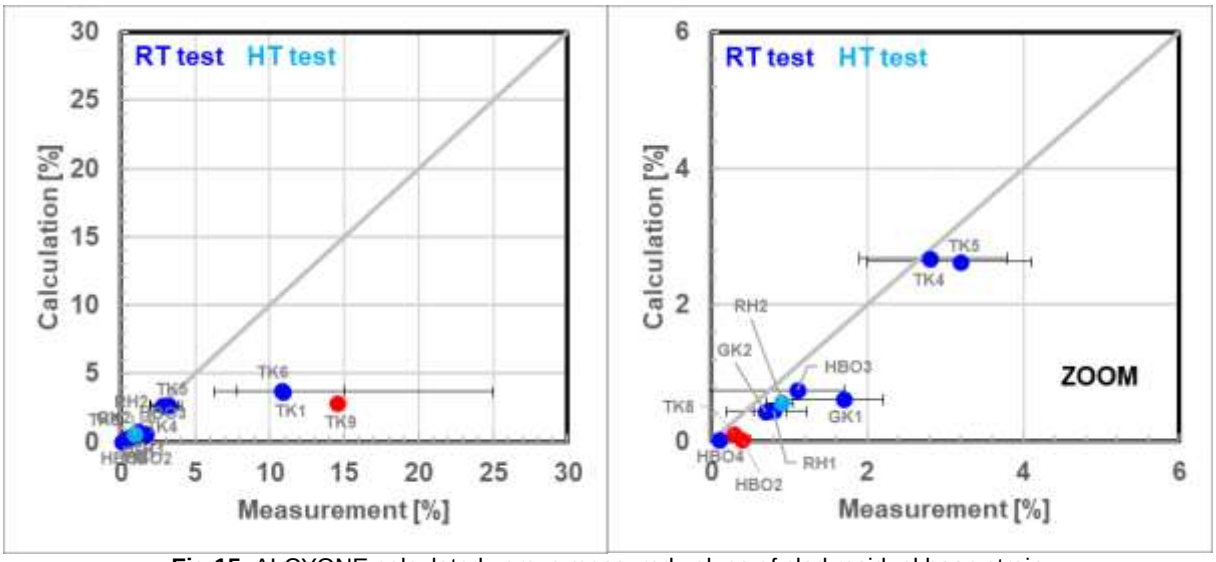

Fig 15. ALCYONE calculated *versus* measured values of clad residual hoop strain (symbols: dark blue for RT test, hell blue for HT test)

The somewhat regular increase of residual hoop strain with peak enthalpy increase below ~600 J/g exhibited in Fig 1 is globally well reproduced by ALCYONE. Beyond 600 J/g, the impact of the high clad temperature on the material behaviour (with a change of slope characteristic of clad ballooning) is not captured in ALCYONE calculations. Improvement is clearly needed on this point.

5. Investigation on the origin of clad ballooning during NSRR RIA tests

The NSRR tests that present significant ballooning are all from the TK-series. Simulations of these tests with ALCYONE showed that the FGR during the transient is correctly reproduced as well as the film boiling duration and the peak clad outer surface temperature. The underestimation of clad hoop strains during the transient cannot therefore be attributed to the modeling of thermal heat exchange and FGR in the code. Simulation trends during the TK-1 test are illustrated in Fig 16. They show that the FGR occurs quasi instantaneously during the power pulse (within 10 ms starting at around 0.242 s) and leads to a rise of the internal pressure till 43 bar (y-axis scale in bar). At this time, the clad temperature is however not sufficient (less than 350°C) to induce significant clad deformation. The pressure quickly decreases once clad deformation starts to increase. Obviously, the maximum pressure reached is not sufficient to induce more than 5% hoop strains during the transient.

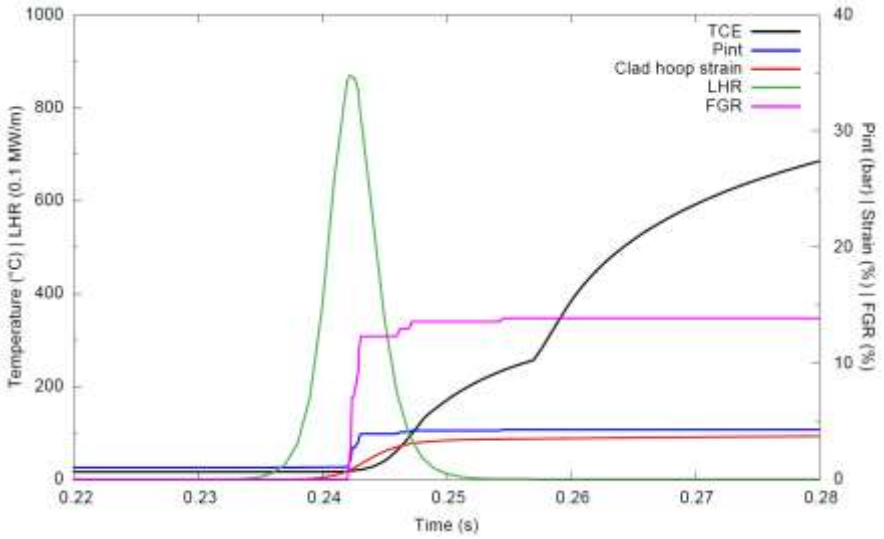

Fig 16. Case TK-1. Pressure equilibrium reference calculation. Time evolution of various physical quantities of interest at peak power level (TCE: clad outer surface temperature; Pint: internal pressure; Gap: radial pellet-clad gap width; LHR; FGR)

It is with the abovementioned needed improvement for clad residual hoop strain simulation in mind that the model for delayed gas axial flow within the fuel rod has been implemented. A permeability of 10E-14 m², consistent with the estimation of reference [61] based on gas flow rate during rod puncturing, has here been used.

Simulation trends during the TK-1 test are again illustrated in **Fig 17** but this time considering that pressure equilibrium does not hold in the rod free volume. The lack of pressure equilibrium in the rod is illustrated in **Fig 18**. As shown in **Fig 17**, the kinetics of FGR and rod pressure evolution are similar than in the previous simulation with however a maximum pressure reaching 360 bar. The residual clad hoop strain increases by a small amount (around 3.5%) but remains far from the local 25% measured after the test. Additional simulations with a decreasing gas permeability in the fuel did not improve the results. The reason being that the clad temperature at the time of the overpressure is not sufficient to allow significant deformations to take place.

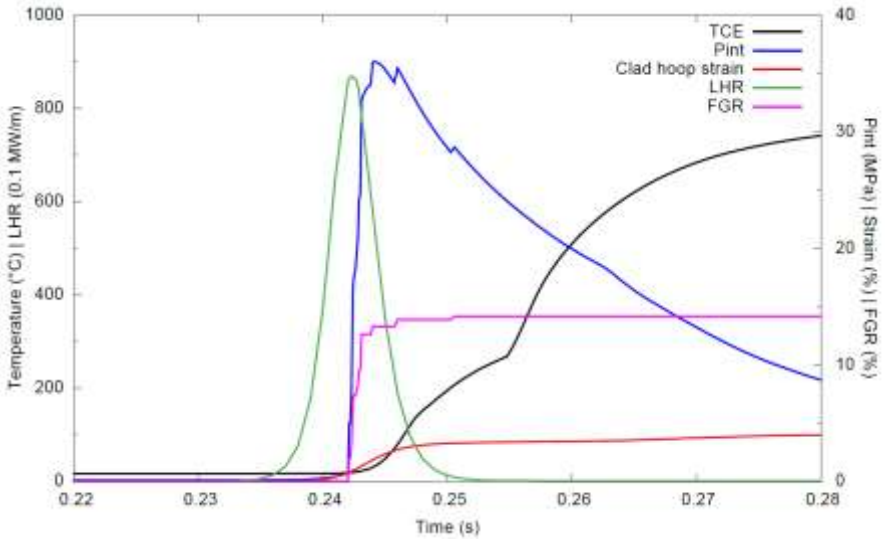

Fig 17. Case TK-1. Calculation with delayed gas axial flow and no time-shift of FGR. Time evolution of various physical quantities of interest at peak power level (TCE: clad outer surface temperature; Pint: internal pressure; Gap: radial pellet-clad gap width; LHR; FGR)

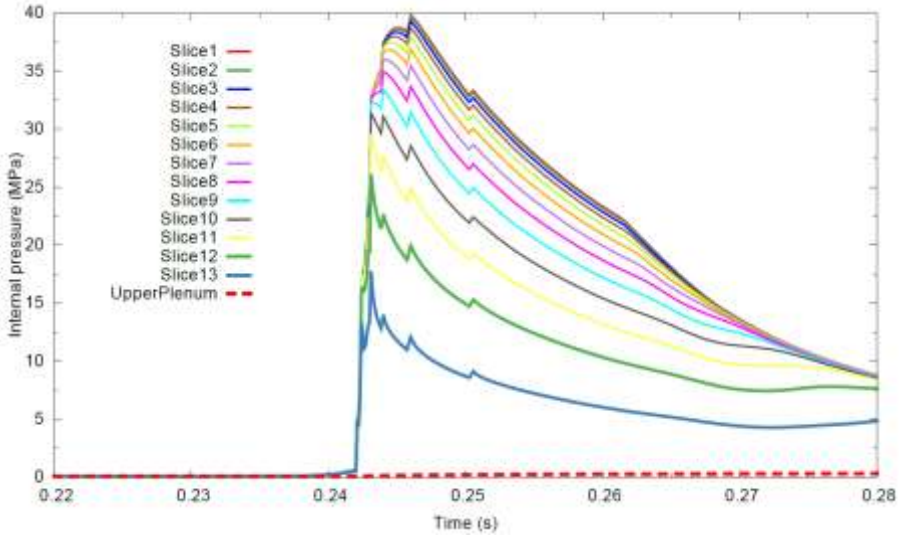

Fig 18. Case TK-1. Calculation with delayed gas axial flow and no time-shift of FGR. Time evolution of internal pressure for each slice and the upper plenum of the rodlet

These simulations clearly evidence the need for a more convenient timing of fission gas release and rod internal pressure increase with respect to the clad temperature elevation. As the latter has already been optimized by a new parameter fitting of the boiling curve, some attempts have been made to artificially time-shift the fission gas release. This is illustrated in Fig 19 on the TK-1 case showing the comparative time evolution of various physical quantities at peak power level when assuming fission gas release occurs at pre-determined times after the start of the test, i.e., 0.3 s (top left), 0.44 s (top right) or 0.5 s (bottom left). The corresponding time evolution of calculated clad hoop strains is plotted in the bottom right graph.

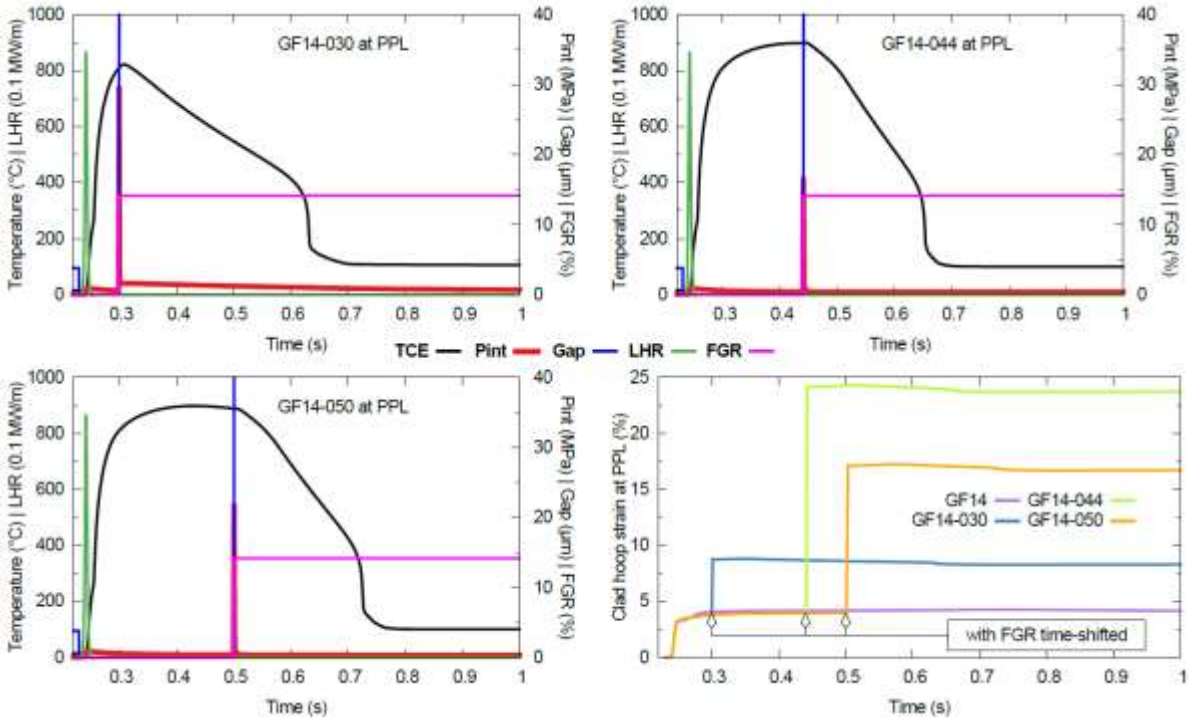

Fig 19. Case TK-1. Calculation with delayed gas axial flow and time-shift of FGR. Illustration of the comparative time evolution of various physical quantities of interest at peak power level (PPL)
(TCE: clad outer temperature; Pint: internal pressure; Gap: radial pellet-clad gap width; LHR: linear heat rate; FGR: fission gas release)

Time-shifting the FGR leads to calculated clad outer temperature *versus* time curves more consistent with the measured ones [16]. In particular, they now exhibit a long plateau at high temperature during the film boiling phase (the same trend can be observed during the TK-6 test [54]). It also affects the film boiling duration, but marginally.

For each of the FGR times, a high peak of internal pressure is obtained, between 18 and 30 MPa (for an initial value of 0.1 MPa before pulse irradiation). This overpressure gives rise to a lasting reopening of the pellet-clad gap and to important clad hoop strains (up to 25%). Clad temperature has an impact on the internal pressure maximum level achieved in each case, as the ballooning tends to mitigate the overpressurization more rapidly when the clad temperature is higher.

This example shows that it is possible to achieve high levels of clad hoop strains, consistent with the TK-1 post-test measurements with residual strains of 25 %, when considering a FGR time 0.44 s which actually corresponds to the occurrence of the peak clad outer surface temperature.

This result brings an alternative explanation to the one given in reference [16] where this ballooning was attributed to pronounced fission gas induced swelling of the fuel and pellet-clad gap was shown to remain closed. It is here considered that the obviously important level of pellet cracking with some pellet fragments stuck to the clad inner surface might have led to the formation of some open gap space-shifted from the natural pellet-clad interface.

The same exercise as for TK-1, aiming at imposing fission gas release simultaneously with the peak clad outer surface temperature, has been repeated for each of the NSRR tests considered in this paper. Results in terms of calculated values of maximum residual hoop strain *versus* peak enthalpy increase are plotted in Fig 20. The experimental change of slope around 600 J/g and the evolution at high enthalpy increase shown in Fig 1 is well reproduced.

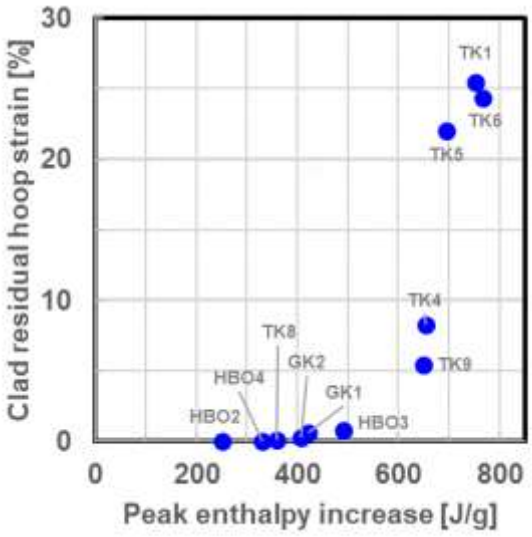

Fig 20. ALCYONE calculated values of axially maximum clad residual hoop strain *versus* peak fuel enthalpy

From the curves of Fig 18, one may note that the time-shifted fission gas release remains globally as instantaneous as the computed one in the reference simulation. Notwithstanding this rough approach, the whole set of results seems consistent and raises expectations that still improved calculated results could be achieved should progressive fission gas release be modeled and implemented in the ALCYONE code. This modeling should account for the gas propagation in open fuel voids (cracks, pores…) before they could be released. The associated permeability of the fuel needs to be defined from appropriate experiments.

6. Conclusions and prospects

A selection of NSRR experiments were simulated with the ALCYONE fuel performance code to assess its capability in assessing clad ballooning occurring in fast transients performed in a water coolant.

This exercise showed that ALCYONE calculation results are in reasonable agreement with measurements performed during or after the NSRR tests. The rodlet thermal behaviour and the transient FGR are satisfactorily captured despite some discrepancy for intermediate values of peak enthalpy increase and some overestimation of film boiling duration. The latter has been improved by a readjustment of the boiling curve parameters. As clad residual hoop strains were mostly underestimated especially at high enthalpy increase, a complementary work using the recently implemented gas flow model induced by axial pressure gradients has been proposed. It has shown that high levels of clad residual hoop strain could be achieved provided a proper timing of fission gas release, rod internal pressure increase and clad temperature elevation is used in the simulations. A progressive release of the fission gas from the fuel could therefore help modeling clad ballooning during the NSRR tests. Work aiming at modeling fission gas release kinetics in a more physical manner is underway including debates on what values of fuel permeability should be used in RIA conditions. In spite of these good results, clad hoop strain simulation might also be improved by the modeling of clad high temperature creep which is currently not available in ALCYONE fuel performance code.

Declaration of competing interest

The authors declare that they have no known competing financial interests or personal relationships that could have appeared to influence the work reported in this paper.

CRediT authorship contribution statement

I. Guénot-Delahaie: Writing - original draft, Writing – review & editing, Conceptualization, Investigation, Software, Visualization. **J. Sercombe**: Writing - original draft, Writing – review & editing, Conceptualization, Methodology, Formal analysis, Validation. **É. Fédérici**: Resources. **C. Bernaudat**: Resources. **R. Largenton**: Resources. **X. Haller**: Resources.

Acknowledgements

The authors are gratefully indebted to JAEA Udagawa-san for providing a list of data and references that helped completing the literature review.

The work described in the present paper has been performed in the continuity of many years of development of the ALCYONE fuel performance code at CEA with the constant financial and technical support of EDF and Framatome. The authors are thankful to the CEA colleagues for their fruitful contribution to the code development and the underlying physical modeling.

Framatome is acknowledged for providing data for RH-1 and RH-2 tests.

Appendix A.

Compiled details about PWR fuel specimens tested and tests performed in NSRR facility with stagnant water coolant [7,8],[11–41].

	Test ID												
	GK-1	**GK-2**	**HBO-2**	**HBO-3**	**HBO-4**	**TK-1**	**TK-4**	**TK-5**	**TK-6**	**TK-8**	**TK-9**	**RH-1**	**RH-2**
Date of the test	03/12/1991	03/17/1992	03/25/1994	10/19/1994	01/24/1995	11/29/1996	02/04/1998	10/01/1998	10/07/1998	11/25/2000	12/25/2000	02/22/2006	n.m.
Power reactor for parent fuel rod irradiation	Genkai 1 Japan	Genkai 1 Japan	Ohi 1 Japan	Ohi 1 Japan	Ohi 1 Japan	Takahama 3 Japan	Takahama 3 Japan	Takahama 3 Japan	Takahama 3 Japan	Takahama 3 Japan	Takahama 3 Japan	Ringhals 4 Sweden	Ringhals 4 Sweden
Parent fuel rod manufacturer	n.m.	n.m.	MHI Ltd	MHI Ltd	MHI Ltd	MHI Ltd	MHI Ltd	MHI Ltd	MHI Ltd	NFI Ltd	NFI Ltd	Framatome	Framatome
Common parent rod with another test if any	-	-	-	-	-	TK-6	-	-	TK-1	-	-	RH-2	RH-1
Fuel rod design and type	14x14 PWR-UO_2	14x14 PWR-UO_2	17x17 PWR-UO_2	17x17 PWR-UO_2	17x17 PWR-UO_2	17x17 PWR-UO_2	17x17 PWR-UO_2	17x17 PWR-UO_2	17x17 PWR-UO_2	17x17 PWR-UO_2	17x17 PWR-UO_2	17x17 PWR-UO_2	17x17 PWR-UO_2
Manufacturing data	Normal grain size	Normal grain size	Normal grain size	Normal grain size	Normal grain size	Normal grain size	Normal grain size	Normal grain size	Normal grain size	Normal grain size	Normal grain size	Normal grain size	Normal grain size
^{235}U initial enrichment (wt%)	3.4	3.4	3.2	3.2	3.2	4.1	4.1	4.1	4.1	4.1	4.1	3.7	3.7
Pu Initial enrichment (wt%)	-	-	-	-	-	-	-	-	-	-	-	-	-
Pellet outer diameter (mm)	9.29	9.29	8.19	8.19	8.19	8.19	8.19	8.19	8.19	8.19	8.19	8.191	8.191
Pellet height (mm)	15.2	15.2	13.5	13.5	13.5	10.0	10.0	10.0	10.0	10.0	10.0	13.5	13.5
Clad initial thickness (mm)	0.62	0.62	0.57	0.57	0.57	0.57	0.57	0.57	0.57	0.57	0.57	0.57	0.57
Clad inner diameter[a] (mm)	9.48	9.48	8.36	8.36	8.36	8.36	8.36	8.36	8.36	8.36	8.36	8.36	8.36
Clad inner diameter[a] (mm)	10.72	10.72	9.5	9.5	9.5	9.5	9.5	9.5	9.5	9.5	9.5	9.5	9.5
Cladding alloy[c]	Zircaloy-4	Zircaloy-4	Zircaloy-4	Zircaloy-4	Zircaloy-4	Low-tin Zircaloy-4	Low-tin Zircaloy-4	Low-tin Zircaloy-4	Low-tin Zircaloy-4	Low-tin Zircaloy-4	Low-tin Zircaloy-4	M5®, RX	M5®, RX
Rodlet active fuel length (mm)	121	121	135	135	135	130	130	110	110	130-135	130-135	117	50
Sampling position from bottom (mm) [span from top]	1618-1744 [3/6]	1435-1603 [3/6]	[4/8]	[5/8]	[6/8]	[5]	[3]	[2]	[3]	[4]	n.a.	1322-1440 [3]	1638-1688
Rodlet fill gas	He	He	He	He	He	He	He	He	He	He	He	He	He
Rodlet fill gas pressure (MPa)	4.3	0.1	5.1	0.1	0.1	0.1	0.1	0.1	0.1	0.1	3	0.1	0.1
Rodlet free volume (cm^3)	1.5[n]	1.5[n]	n.a.	n.a.	n.a.	n.a.	n.a.	n.a.	n.a.	n.a.	n.a.	4	1
Base irradiation number of cycles	3	3	4	4	4	2	3	3	2	3	3	5	5
LHGR at last cycle (kW/m)	19.8	19.8	15.4	15.4	15.4	n.a.	n.a.	n.a.	n.a.	n.a.	n.a.	16.	16.
LHGR mean/max over base irradiation (kW/m)	20.2/n.m.	20.2/n.m.	15.5/19.5	15.5/19.5	15.5/19.5	19./20.5	19./20.5	19./20.5	19./20.5	19./20.5	19./20.5	20.5/26.	20.5/26.
Local burnup (GWd/tM)	42.1	42.1	50.4	50.4	50.4	38	50	48	38	50	50	67	67
Clad corrosion thickness (µm)	10	10	30 - 40	20 - 25	15 - 20	7	25	30	15	10	< 10	6[e]	6[e]
Clad hydrogen concentration[d] (wtppm)	n.a.	n.a.	152	148	89	50	125	163	100	n.a.	n.a.	70	70
FGR during base irradiation (%)	0.76	0.76	0.49	0.49	0.49	< 0.4	< 0.4	< 0.4	< 0.4	< 0.4	< 0.4	2.4	2.4
Capsule type	RT	RT	RT	RT	RT	RT	RT	RT	RT	RT	RT	RT	HT
Sibling RT/HT test if any	-	-	-	-	-	-	-	-	-	-	-	RH-2	RH-1
Initial coolant temperature[f] (°C)	21	21	20	20	20	20	20	20	20	20	20	16	278
Coolant pressure (MPa)	0.1	0.1	0.1	0.1	0.1	0.1	0.1	0.1	0.1	0.1	0.1	0.1	6.4
Pulse width (FWHM) (ms)	4.6	4.6	6.9	4.4	5.3	4.4	4.4	4.4	4.4	7.0	4.4	4.4	4.5
Energy deposit J/g_{fuel}	506	490	213	397	280	674	523	544	669	351	527	510	481
Max. pellet stack axial elongation (mm)	1.28	0.72	0.6[p]	n.a.	0.8	2.25	n.a.	n.a.	1.9	n.a.	n.a.	n.a.	n.a.
Max. cladding tube axial elongation (mm)	1.16	0.27	0.5	n.a.	0.6	2	n.a.	n.a.	1.6	n.a.	n.a.	n.a.	n.a.
Peak fuel enthalpy[b] J/g_{fuel}	421	407	252	490	330	753	654	694	768	359	649	462	447
Initial fuel enthalpy (at 20°C) J/g_{fuel}	0	0	0	0	0	0	0	0	0	0	0	0	69
Peak fuel enthalpy increase[g] J/g_{fuel}	421	407	252	490	330	753	654	694	768	359	649	462	378

DNB detection	yes	yes	no	yes	no	yes	no	no	yes	no	no	yes	yes[h]
Clad outer surface temperature[m] (K) max. min.	581	569	395	673	385	860 493	873	873	980 653	n.a.	n.a.	429 346	942
Film boiling duration (s) max. min.	0.4	0.3	-	0.3 0.1	-	1.05 0.35	-	-	1.5 0.4	-	-	0.06	2.35
Clad residual hoop strain[i] (%) max.[j] mean min.	2.2 1.7 0.9	1.1 0.7 0.2	0.4 n.a. n.a.	1.5 1.1 0.5	0.2 0.1 0.	25 10.9 6.3	3.8 2.8 1.9	4.1 3.2 2.	15.5 10.8 7.8	0.3	14.6	0.96[j] 0.8 0.6	1.06[j] 0.91 0.7
Transient FGR[o] (%)	11.7[l]	7.0	17.7	22.7	21.1	20	8.3	11.1	16.2	5.9[l]	6.2	21.4	26.0
Profilometry results	[29]	[29]		[27]	[27]	[16]	[16]	[16]	[16]			[9]	[9]
Metallography results	[29]	[29]	[31]	[31][37][38]	[31]	[16]						[9]	[9]
Temperature time evolution results	[29]	[29]	[38]	[54][27]		[16]			[54]			[9]	[9]
Inner pressure time evolution results						[40]			[40]		[39]		

n.m. = not measured or not mentioned; n.a. = not available; normal grain size = around 10 µm.
MIMAS AUC = MIcronised MASter blend, Ammonium Urano-Carbonate (fabrication technology); LHGR = Linear Heat Generation Rate; DNB = Departure from Nucleate Boiling; RX = recrystalised; SR = stress-relieved.
RT and HT stand for « Room-Temperature, Atmospheric-Pressure » and « High-Temperature, High-Pressure » respectively.
[a] nominal value.
[b] radial average.
[c] chemical composition – (standard) Zircaloy-4: Zr-1.5Sn-0.2Fe-0.1Cr by wt%; low-tin Zircaloy-4: Zr-1.3Sn-0.2Fe-0.1Cr by wt%
[d] estimated relative uncertainty: less than 3% [8]
[e] estimated absolute uncertainty: less than 1 µm [8]
[f] estimated absolute uncertainty: less than 3 K [8]
[g] evaluation based on the total amount of fissile materials in a tested rod and computation by the neutron transport calculation model for the NSRR core. Estimated relative uncertainty: about 7% [6][8]
[h] but no stable film boiling [9]
[i] azimuthally averaged.
[j] maximum clearly located at mid-pellets (barrel-shape pellets).
[k] disregarding end pellets.
[l] absolute uncertainty of 2%, accounting for variability of published data.
[m] disregarding any smoothing of available curves; potential undermeasurement by 200-300 K [60]
[n] uncertainty multiplying factor of 1.6, accounting for variability of available data.
[o] highly fragmented end pellets if any may contribute a lot to measured transient FGR.
[p] indication of rigid adhesion between the fuel pellets and the clad.

Clad outer surface peak temperature and film boiling uncertainty sources:
HBO-3 – Axial variability – Results for 2 TCs – DNB for 2 TCs – Film boiling only for TC located 40 mm below pellet stack center.
TK-1 (same burnup and enthalpy level as TK-6) – Axial variability – Results for 3 TCs – DNB for 3 TCs – Film boiling only for TCs located 42 mm (highest peak temperature) and 2 mm below pellet stack center.
TK-6 (same burnup and enthalpy level as TK-1) – Axial variability – Results for 3 TCs – Film boiling for 3 TCs – Highest peak temperature reached for TC located 42 mm above pellet stack center.
RH-1 – Axial variability – Results for 3 TCs – DNB only for 2 TCs – No stable film.

REFERENCES

1. J. Sercombe et al., “Modeling of pellet cladding interaction”, in: *Compr. Nucl. Mater. 2nd*, pp. 417-465, R. Konings and R. Stoller Eds, Elsevier Ltd (2020).
2. J. Sercombe et al., “1D and 3D modeling of PCMI during a RIA with ALCYONE V1.1”, *Proc. of TopFuel Conference,* Orlando, Florida, USA (2010).
3. J. Sercombe et al., “2D simulation of hydride blister cracking during a RIA transient with the fuel code ALCYONE”, *EPJ Nuclear Sci. Technol.*, **2**, 22 (2016).
4. I. Guénot-Delahaie et al., “Simulation of RIA transients on UO_2-M5® fuel rods with ALCYONE V1.4 fuel performance code”, *Nucl. Eng. Technol.,* **50***,* 268 (2018).
5. I. Guénot-Delahaie et al., “Simulation of RIA transients on MOX fuel rods with ALCYONE fuel performance code”, *Proc. of TopFuel Conference,* Prague, Czech Republic (2018).
6. B. Biard et al., “Reactivity Initiated Accident transient testing on irradiated fuel rods in PWR conditions: The CABRI International Program”, *Annals of Nucl. Energy*, **141**, article 107253 (2020).
7. Y. Udagawa et al., “Reevaluation of fuel enthalpy in NSRR test for high burnup fuels”, *Proc. of Water Reactor Fuel Performance Meeting/TopFuel Conference*, Sendai, Japan (2014).
8. Y. Udagawa et al., “Thresholds for failure of high-burnup LWR fuels by Pellet Cladding mechanical interaction under reactivity-initiated accident conditions”, *J. Nucl. Sci. Technol.*, **56**, 1063 (2019).
9. “Nuclear fuel behaviour under reactivity-initiated accident (RIA) conditions: updated state-of-the-art report”, NEA/CSNI, Nuclear Energy Agency, Organisation for Economic Co-operation and Development (to be released, 2021).
10. “WGFS RIA Fuel Rod Codes Benchmark Phases 1-3 Synthesis Report”, NEA/CSNI, Nuclear Energy Agency, Organisation for Economic Co-operation and Development (to be released, 2021).
11. A. Sakurai et al., “Correlations for subcooled pool film boiling heat transfer from large surfaces with different configurations”, *Nucl. Eng. Des.*, **120**, 271 (1990).
12. T. Sugiyama et al., “Evaluation of initial temperature effect on transient fuel behavior under simulated reactivity-initiated accident conditions”, *J. Nucl. Sci. Technol.*, **47**, 439 (2010).
13. T. Sugiyama, “Applicability of NSRR Room/High Temperature test results to fuel safety evaluation under power reactor conditions”, *OCDE/NEA workshop on nuclear fuel behaviour during Reactivity Initiated Accidents*, Paris, France (2009).
14. Y. Udagawa et al., “Experimental and analytical study on MOX fuel behavior under RIA-simulating conditions in the NSRR”, *IAEA-TM on Fuel design and licensing of mixed cores for water cooled reactors*, Vienna, Austria (2011).
15. T. Fuketa et al., “Fuel failure and fission gas release in high burnup PWR fuels under RIA conditions”, *J. Nucl. Mater.*, **248**, 249 (1997).
16. T. Fuketa et al., “Behavior of high-burnup PWR fuels with low-tin Zircaloy-4 cladding under reactivity-initiated-accident conditions”, *Nucl. Technol.*, **133**, 50 (2001).
17. M. Amaya et al., “Behavior of high burnup advanced fuels for LWR during design-basis accidents”, *Proc. of TopFuel Conference*, Zurich, Switzerland (2015).
18. T. Fuketa et al., “Behaviour of high burnup PWR fuels during simulated reactivity-initiated accident conditions”, *Proc. of TopFuel Conference*, Salamanca, Spain (2006).
19. M. Amaya et al., “Behavior of high burnup advanced LWR fuels under accident conditions”, *Proc. of TopFuel Conference*, Boise, Idaho, USA (2016).
20. T. Fuketa et al., “Behavior of high burnup LWR fuels during design-basis accidents; key observations and an outline of the coming program”, *Proc. of TopFuel Conference*, Orlando, Florida, USA (2010).

21. Y. Udagawa et al., “Recent research activities using NSRR on safety related issues”, *Proc. of ICAPP conference*, San Francisco, California, USA (2016).
22. K. Tomiyasu et al., “Influence of cladding-peripheral hydride on mechanical failure under reactivity-initiated accident conditions”, *J. Nucl. Sci. Technol.*, **44**, 733 (2007).
23. T. Sugiyama et al., “Failure of high burnup fuels under reactivity-initiated accident conditions”, *Annals of Nucl. Energy*, **36**, 380 (2009).
24. T. Fuketa et al., “Fuel failure and fission gas release in high burn-up PWR fuels under RIA condition”, *J. Nucl. Mater.*, **248**, 249 (1997). .
25. T. Fujishiro et al., “Transient fuel behaviour of preirradiated PWR fuels under RIA conditions”, *J. Nucl. Mater.*, **188**, 162 (1992).
26. T. Nakamura et al., “NSRR RIA test results and experimental programmes", *Proc. of the topical meeting on RIA fuel safety criteria*, Aix-en-Provence, France (2002). (NEA/CSNI/R(2003)8/vol. 2)
27. T. Fuketa et al., “NSRR/RIA experiments with high burnup PWR fuels”, *Nucl. Safety*, **37**, 328 (1996).
28. M. Amaya et al., “Behavior of high burnup advanced LWR fuels under design-basis accident conditions”, *Proc. of Water Reactor Fuel Performance Meeting/TopFuel Conference*, Jeju Island, Korea (2017).
29. H. Sasajima et al., “Behavior of irradiated PWR fuel under simulated RIA conditions - Results of the NSRR tests GK-1 and GK-2”, *JAERI Research 2004-022* (2004).
30. M. Amaya et al., “Behavior of high-burnup LWR fuels with improved materials under design-basis accident conditions”, *Proc. Of TopFuel Conference*, Prague, Czech Republic (2018).
31. H. Sasajima et al., “Fission gas release behavior of high burnup UO_2 fuel under reactivity initiated accident conditions”, *J. Nucl. Sci. Technol.*, **36**, 1101 (1999).
32. H. Sasajima et al., “Identification of radial position of FGR in HBU pellets under RIA conditions”, *J. Nucl. Sci. Technol.*, **47**, 202 (2010).
33. T. Fuketa et al., “NSRR experiment with 50 MWd/kgU PWR fuel under an RIA condition”, *Proc. of TCM*, Dimitrovgrad, Russia, (1995). (IAEA-TECDOC-921)
34. T. Nakamura et al., “Fission gas induced cladding deformation of LWR fuel rods under RIA conditions”, *J. Nucl. Sci. Technol.*, **33**, 924 (1996).
35. T. Sugiyama et al., “Mechanical energy generation during High burnup fuel failure under RIA conditions”, *J. Nucl. Sci. Technol.*, **37**, 877 (2000).
36. T. Fuketa et al., “Behaviour of LWR/MOX fuels under reactivity-initiated accident conditions”, *Proc. of TopFuel conference*, Paris, France (2009).
37. T. Fuketa et al., *Proc. 23rd Water Reactor Safety Information Meeting*, Bethesda, Maryland USA (1995), NUREG/CP-0149, Vol. 1 (USNRC, 1996).
38. T. Fuketa et al., “Behavior of High Burnup PWR Fuel Under a Simulated RIA Condition in the NSRR”, *Proc. of CSNI Specialist Meeting on Transient Behavior of High Burnup Fuel*, Cadarache, France (1995), NEA/CSNI/R(95)22 (OECD/NEA 1996).
39. T. Nakamura et al., “NSRR RIA tests on PWR, BWR and MOX fuels”, *Proc. of Fuel Safety Research Specialists’ Meeting*, *JAERI-Conf. report 2002-009* (2002).
40. É. Fédérici, “The SCANAIR code version 3.2 - Application to the interpretation of the NSRR TK1 test”, *Proc. of 24th NSRR technical review meeting*, *JAERI-Conf. report 2001-010* (2001).
41. Y-H. Koo et al., “Artificial neural network modeling for FGR in LWR UO_2 fuel under RIA conditions”, *J. Nucl. Mater.*, **405**, 33 (2010).
42. Cast3M. Available at: http://www-cast3m.cea.fr/.
43. B. Cazalis et al., “The PROMETRA program: fuel cladding mechanical behavior under high strain rate”, *Nucl. Technol.,* **157**, 215 (2007).
44. B. Cazalis et al., “The PROMETRA program: a reliable material database for highly irradiated zircaloy-4, ZIRLO™ and M5™ fuel claddings”, *Proc. of SMiRT18 Conference*, Beijing, China (2005).

45. B. Cazalis et al., "The PROMETRA program: plane strain tests on fresh and highly irradiated Zircaloy-4, ZIRLO® and M5™ fuel claddings", *Proc. of TopFuel Conference*, Boise, Idaho, USA (2016).
46. M. Le Saux et al., "A model to describe the anisotropic viscoplastic mechanical behavior of fresh and irradiated Zircaloy-4 fuel claddings under RIA loading conditions", *J. Nucl. Mater.*, **378**, 60 (2008).
47. A. Moal et al., "SCANAIR a transient fuel performance code. Part two: General modelling description", *Nucl. Eng. Des.*, **280**, 150 (2014).
48. V. Marelle, "Validation of PLEIADES/ALCYONE 2.0 fuel performance code", *Proc. of Water Reactor Fuel Performance Meeting/TopFuel Conference*, Jeju Island, Korea (2017).
49. M. Salvo et al., "Experimental characterization and modeling of UO_2 behavior at high temperatures and high strain rates, *J. Nucl. Mater.*, **456**, 54 (2015).
50. M. Salvo et al., "Experimental characterization and modeling of UO_2 grain boundary cracking at high temperatures and high strain rates, *J. Nucl. Mater.*, **460**, 184 (2015).
51. G. Jomard et al., "CARACAS: an industrial model for description of fission gas behavior in LWR-UO_2 fuel", *Proc. of Water Reactor Fuel Performance Meeting/TopFuel Conference*, Sendai, Japan (2014).
52. J.-P. Hiernaut et al., "Fission product release and microstructure changes during laboratory annealing of a very high burn-up fuel specimen", *J. Nucl. Mater.*, **377**, 313 (2008).
53. V. Bessiron, "Modelling of clad-to-coolant heat transfer for RIA applications", *J. Nucl. Sci. Technol.*, **44**, 211 (2007).
54. V. Bessiron et al., "Clad-to-coolant heat transfer in NSRR experiments", *J. Nucl. Sci. Technol.*, **44**, 723 (2007).
55. Reactivity initiated accident (RIA) fuel codes benchmark Phase-II, Report – Volume 1, Simplified cases results, Summary and analysis, NEA/CSNI/R(2016)6/VOL1, Nuclear Energy Agency, Organisation for Economic Cooperation and Development (2016).
56. V. Georgenthum et al., "SCANAIR a transient fuel performance code. Part two: Assessment of modelling capabilities", *Nucl. Eng. Des.*, **280**, 172 (2014).
57. T. Sugiyama et al., "Effect of cladding surface pre-oxidation on rod coolability under reactivity initiated accident conditions", *J. Nucl. Sci. Technol.*, **41**, 7 (2004).
58. RIA Fuel Codes Benchmark – Volume 1, NEA/CSNI/R(2013)7, Nuclear Energy Agency, Organisation for Economic Co-operation and Development (2013).
59. Y. Muramatsu et al., "Post-Irradiation Examination and In-pile Measurement Techniques for Water Reactor Fuels", *IAEA-TECDOC-CD-1635*, IAEA, Vienna (2009).
60. T. Tsuruta et al., "Evaluation of thermocouple fin effect in cladding surface temperature measurement during film boiling", *J. Nucl. Sci. Technol.*, **21**, 7 (1984).
61. R. Montgomery, R. N. Morris, "Measurement and modeling of the gas permeability of high burnup pressurized water reactor fuel rods", *J. Nucl. Mater.*, **523**, 206 (2019).